

Article

# Effects of Polydopamine Incorporation on the Nanostructure and Electrochemical Performance of Electrodeposited Polypyrrole Films

James A. Behan \* and Frédéric Barrière 

Université de Rennes, CNRS, UMR 6226, Institut des Sciences Chimiques de Rennes, 35042 Rennes, France; frederic.barriere@univ-rennes.fr

\* Correspondence: james.behan@univ-rennes.fr

**Abstract:** Polypyrrole films are commonly prepared as conductive electrode surfaces for a variety of applications. Recently, there has been increasing interest in improving the adhesive properties and biocompatibility of polypyrrole electrodes via the incorporation of bioinspired polydopamine within the polymer scaffold. However, very little is currently known about the structural effects of polydopamine incorporation during the electropolymerisation of hybrid films. In this work, we combine electrochemical quartz crystal microbalance studies, fundamental electrochemical characterisation, atomic force microscopy, and a suite of spectroscopic techniques in order to correlate changes in the structure and performance of polypyrrole–polydopamine films to the structural modifications of the nanostructure induced by polydopamine incorporation. The results indicate that polydopamine incorporation greatly increases the rate of hybrid film deposition, as well as improving adhesion, surface homogeneity, and wettability, with no compromise in charge transfer properties. Polydopamine incorporation is strongly suggested to occur in non-connected domains within a predominantly polypyrrole-like scaffold. We propose a two-step model of co-polymerisation and the subsequent surface adhesion of hybrid films. Results are expected to be of broad general interest to researchers utilizing polypyrrole and polydopamine to prepare tailor-made electrodes for biosensing and catalysis.

**Keywords:** carbon nanostructure; electrodeposition; dopamine; polydopamine; polypyrrole; optoelectronics; surface chemistry



**Citation:** Behan, J.A.; Barrière, F. Effects of Polydopamine Incorporation on the Nanostructure and Electrochemical Performance of Electrodeposited Polypyrrole Films. *C* **2024**, *10*, 20. <https://doi.org/10.3390/c10010020>

Academic Editor: Patrizia Savi

Received: 15 January 2024

Revised: 6 February 2024

Accepted: 14 February 2024

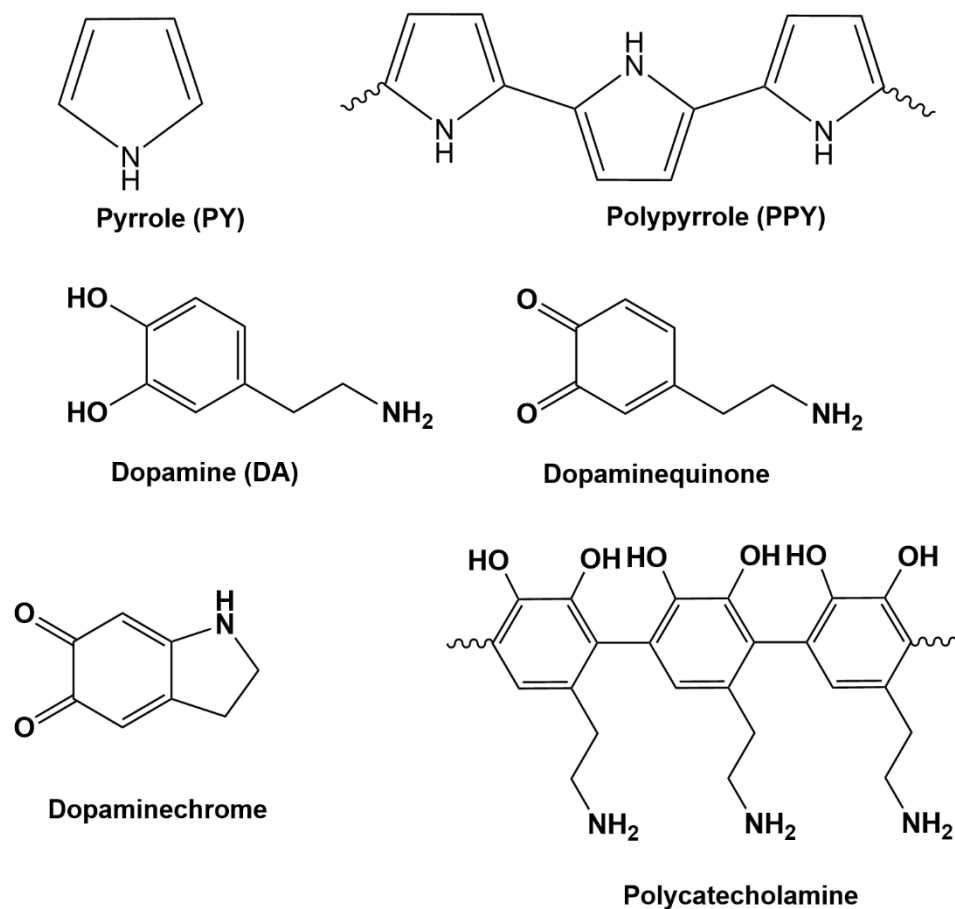
Published: 20 February 2024



**Copyright:** © 2024 by the authors. Licensee MDPI, Basel, Switzerland. This article is an open access article distributed under the terms and conditions of the Creative Commons Attribution (CC BY) license (<https://creativecommons.org/licenses/by/4.0/>).

## 1. Introduction

Polypyrrole (PPY) is the best-investigated poly-heterocyclic polymer owing to its low cost, ease of preparation and modification, and unique semiconducting/metallic properties [1,2]. PPY has been applied in a vast array of applications in biocompatible coatings [3,4], flexible supercapacitors [5,6], and biosensors [7,8], and as carbon support materials in fuel cell devices [9,10]. Recently, several groups have explored the co-deposition of PPY films with dopamine (DA) to form polydopamine (PDA) in order to impart favourable properties such as biocompatibility [11] and greater adhesion across a variety of substrates [12]. PDA is a well-known bioinspired material which, like PPY, is facile to deposit and has been proposed for myriad applications in domains ranging from biotechnology to energy [13–17]. The structure of PDA is highly complex, but is generally thought to comprise subunits rich in (poly)catecholamines, (poly)dopaminequinone, and (poly)dopaminechrome-like subunits [13]. Scheme 1 summarises monomeric and polymeric species relevant to this work.



**Scheme 1.** Illustration of relevant monomeric and polymeric species in PPY-PDA film formation.

Research in hybrid polypyrrole–polydopamine (PPY-PDA) films has to date been largely phenomenological in nature, i.e., PPY-PDA films have been prepared using different ratios of each monomer and the performance of the resulting materials has been characterised in the context of improved adhesion [18] or biocompatibility [11]. However, to our knowledge, a systematic evaluation of the nature of PDA incorporation on the nanostructure of PPY has not been carried out, despite the great potential of these hybrid materials as tunable electrode materials with tailored electrochemical and interfacial properties.

In this work, we prepared PPY-PDA hybrid films in neutral pH buffer via electrodeposition on a variety of electrode surfaces and characterized them using a suite of physicochemical and spectroscopic techniques. Neutral pH was chosen as a mild, biocompatible condition under which electroless polymerisation of PDA due to  $O_2$  oxidation and subsequent cyclisation reactions should still be limited. We showed via in situ electrochemical quartz crystal microbalance (eQCM) measurements that the presence of DA during electrodeposition greatly enhances the growth rate of hybrid PPY-PDA films, even at lower applied electrode potentials. Spontaneous deposition of PDA under our chosen experimental conditions was also ruled out using these methods, suggesting that the enhanced growth rate of PPY-PDA should instead be attributed to the incorporation of PDA or PDA-like regions into the growing PPY film. Unlike PDA films which are well known to block electrodes against charge transfer, PPY-PDA films were found to remain conductive with similar charge-transfer kinetics to hexacyanoferrate(III) as a test redox probe. Atomic force microscopy studies of each film show that PDA incorporation results in a more homogeneous surface than PPY alone, with no evidence of large agglomerates of deposited material. Contact angle analysis of each surface also shows improved wettability for PPY-PDA, which may be attributed both to the surface structure and the presence of

abundant C-O groups from catechol-like moieties introduced into the PDA-like domains of the hybrid film.

To explain these properties of PPY-PDA films, we demonstrate through a combination of X-ray photoelectron spectroscopy (XPS), and other spectroscopic techniques including FTIR, Raman, and UV-visible spectroscopy, that these hybrid PPY-PDA films show a predominantly PPY-like character, with modifications in the nanostructure of the polymer introduced by PDA. PDA incorporation as a minor component during electropolymerisation preserves the overall bulk optoelectronic properties of PPY, preserving its charge transfer properties and optical band gap relative to pure PPY films. We propose a simple 2-step model for PPY-PDA electrodeposition which involves the initial formation of PDA oligomeric building blocks, such as polycatecholamines and polydopaminechrome, which in turn serve as abundant cross-linking sites for the developing PPY scaffold. In this way, favourable adhesive and morphological aspects of PDA films are imparted to the PPY film without compromising its conductivity. Our results are of high relevance to the development of tailored electrode surfaces for applications in catalysis, biosensing, and biotechnology.

## 2. Materials and Methods

### 2.1. Chemicals and Materials

Dopamine hydrochloride (98%), potassium chloride (99.5%), sodium chloride (99%), potassium hexacyanoferrate(III) (>99%), sulphuric acid (>95%, Ultratrace), potassium hydroxide (>99.95%, trace metals basis), sodium phosphate monobasic monohydrate (>98%), and sodium phosphate dibasic (>99%) were purchased from Aldrich (Saint Quentin-Fallavier, France) and used without further purification. Pyrrole (98% reagent grade) was purchased from Aldrich (Saint Quentin-Fallavier, France), purified via distillation, and stored under Ar in aliquots in glass vials at  $-20\text{ }^{\circ}\text{C}$  prior to use. Gold-coated silicon wafer (Au/Si) substrates of 10 nm in size were purchased from Merck and cut to the required dimensions using a diamond scribe prior to use.

### 2.2. Electrochemical and Electrochemical Quartz Crystal Microbalance Studies

Electrochemical experiments were carried out using a potentiostat (Autolab AUT50324, Metrohm, Zofingen, Switzerland) via a three-electrode setup. The reference electrode was an Ag/AgCl electrode (saturated KCl, +197 mV vs. SHE). Graphite rods were used as counter electrodes and a separate counter was used for experiments with PPY and those using PDA to avoid possible cross-contamination due to dopamine intercalation at the graphitised carbon interface [19]. Working electrodes were either glassy carbon or gold disc electrodes ( $0.196\text{ cm}^2$  working area), Au deposited on silicon (Au/Si,  $1.0\text{ cm}^2$  working area), or ITO glass electrodes ( $1.0\text{ cm}^2$  working area) with contacts fabricated in-house and a working area limited using Teflon<sup>®</sup> tape. In the case of eQCM studies, a QCM (Seiko EG&G QCM922A, Seiko, Toyko, Japan) was used along with gold-coated quartz crystal microbalance chips (QA-A9M-AU(M)-25, 9.14 MHz frequency), which were connected externally as working electrodes to the potentiostat.

### 2.3. Preparation of PPY, PDA and PPY-PDA Films

PPY films were deposited via cyclic voltammetry in the potential window 0 to 0.8 V vs. Ag/AgCl (KCl sat) or potentiostatically with a fixed potential of +0.85 V vs. Ag/AgCl (KCl sat). PDA films were deposited using cyclic voltammetry between  $-0.8\text{ V}$  and  $+0.8\text{ V}$  vs. Ag/AgCl (KCl sat) at scan rate of  $50\text{ mV s}^{-1}$ . In all cases, the electrolyte was composed of PBS at pH 7 unless otherwise specified. Solutions were prepared by dissolving dopamine hydrochloride in buffer before adding the required quantity of PY to a final concentration of 150 mM and vortexing to homogenise. The solutions were then degassed for 20 min using Ar and a blanket of Ar gas was retained over the electrolyte throughout the experiment. The DA/PY mole ratio was always kept at 20% as this value was found to produce PPY-PDA films with excellent adhesive properties on a variety of electrode surfaces (*vide infra*). The

post-deposition electrochemical characterisation of films was carried out in solutions of 5 mM potassium hexacyanoferrate(III) in 0.5 M KCl in the potential range of  $-0.2$  to  $+0.6$  V vs. Ag/AgCl (KCl sat) at a scan rate of  $10 \text{ mV}\cdot\text{s}^{-1}$ .

#### 2.4. Characterisation of PPY, PDA and PPY-PDA Films

Atomic force microscopy (AFM) measurements were carried out in tapping mode using an AFM (Ntegra, NT-MDT, Paris, France) with NSG03 tips with a resonant frequency of 47–150 kHz. Images were analysed using open-source software (Gwyddion<sup>®</sup> version 2.65) using the following data processing operations: *level data by mean plane subtraction*, *shift mean value to zero*, and *correct horizontal scars (strokes)*. Profilometry was carried out on PPY and PPY-PDA films using a profilometer (Bruker Dektak XT, Bruker, Palaiseau, France). Films were deposited on Au/Si or ITO glass with the deposition area defined via PTFE tape. Step-edge measurements across a lateral distance of 0.5 mm were used to estimate the thickness of deposited films. FTIR spectra of films on Au/Si substrates were taken using a spectrometer (Vertex 70<sup>®</sup>, Bruker, Marne-la-Vallee, France) using a resolution of  $2 \text{ cm}^{-1}$  and 128 scans per sample. Unmodified Au/Si electrodes were used as reference samples. Raman spectra were taken using a spectrometer (LabRAM HR Evolution, Horiba Scientific, Palaiseau, France) using a  $\times 100$  objective with a 523 nm laser. Two accumulations with acquisition times of 60 s were used for spectra in the range of  $300\text{--}1800 \text{ cm}^{-1}$ . UV-vis measurements of films deposited on ITO glass were taken with a spectrophotometer (V-630 BIO, Jasco, Lisses, France). Water contact angles were measured in triplicate using a contact angle analyser (EasyDrop<sup>®</sup>, KRUSS, Hamburg, Germany) and analysed with open-source software (OpenDrop v3.3.1). XPS data were obtained with a spectrometer (NEXSA G2, ThermoFisher Scientific, Saint-Herblain, France) using an Al K $\alpha$  X-ray source working at 1486.6 eV with a spot size of  $200 \mu\text{m}^2$ , as previously reported [20]. Survey spectra (0–1000 eV) were acquired with an analyzer pass energy of 200 eV (1 eV/step); high-resolution spectra used a pass energy of 50 eV (0.1 eV/step).

#### 2.5. Estimation of Film Thicknesses from eQCM Frequency Data

Film thicknesses were estimated using the Sauerbrey equation and its related parameters, as described in reference [21]:

$$\Delta f = x = \frac{-2f_0^2}{A\sqrt{\rho_q\mu_q}}\Delta m$$

where  $\Delta f$  is the change in frequency,  $\Delta m$  is the change in mass,  $f_0$  is the resonant frequency of the fundamental mode of the QCM chip,  $A$  is the piezoelectrically active area of the quartz crystal ( $0.196 \text{ cm}^2$ ),  $\rho_q$  is the quartz crystal density ( $2.648 \text{ g/cm}^3$ ), and  $\mu_q$  is the shear modulus of the quartz ( $2.947 \times 10^{11} \text{ g/cm}\cdot\text{s}^2$ ). Assuming a density of  $1.5 \text{ g/cm}^3$  for PPY and PPY-PDA films [22] and uniform film coverage, the film thickness was then estimated by dividing the areal mass,  $\Delta m/A$ , by this density.

### 3. Results

#### 3.1. Electrodeposition of Polydopamine-Polypyrrole Films by Cyclic Voltammetry

PPY deposition in the presence of DA was first investigated via cyclic voltammetry (CV). Typical depositions by CV on gold–silicon wafers are shown in Figure 1. PPY-only depositions (Figure 1a) show largely featureless CVs with an onset of oxidation and resulting polymerisation around 0.75 V vs. Ag/AgCl on the first scan, with both Faradaic and capacitive currents increasing on subsequent scans as the deposited PPY film grows. CVs of PPY-PDA films (Figure 1b) show a series of redox peaks in the range between  $-0.4$  to  $+0.4$  V, as well as an earlier onset for oxidative polymerisation at ca. 0.5 V. The redox peaks appear in a similar potential range to those observed for pure polydopamine electropolymerisation by cyclic voltammetry in the range  $-0.8$  V to  $+0.8$  V vs. Ag/AgCl (KCl sat) (Supporting Information Figure S1a) and this can be ascribed to dopamine/dopaminequinone oxidation. Previously, dopamine has been observed to lower

the apparent onset potential of electrodeposition and improve the adhesive properties of the resulting films, even when present in molar ratios of DA:PPY as low as 10% [12]. Here, we observed that PPY-PDA film deposition was more facile (i.e., more rapid, with the coating deposition initiated at lower applied potentials) and produced uniform and coherent coatings on a range of substrates, including indium-tin oxide (ITO) glass (Figure S2a, with voltammetry studies presented in Figure S3), gold (Figure S2b), and glassy carbon (GC, *vide infra*). These experiments led us to conclude that DA incorporation is a robust strategy for preparing conductive and redox-active electrode surfaces on a variety of electrode surfaces.

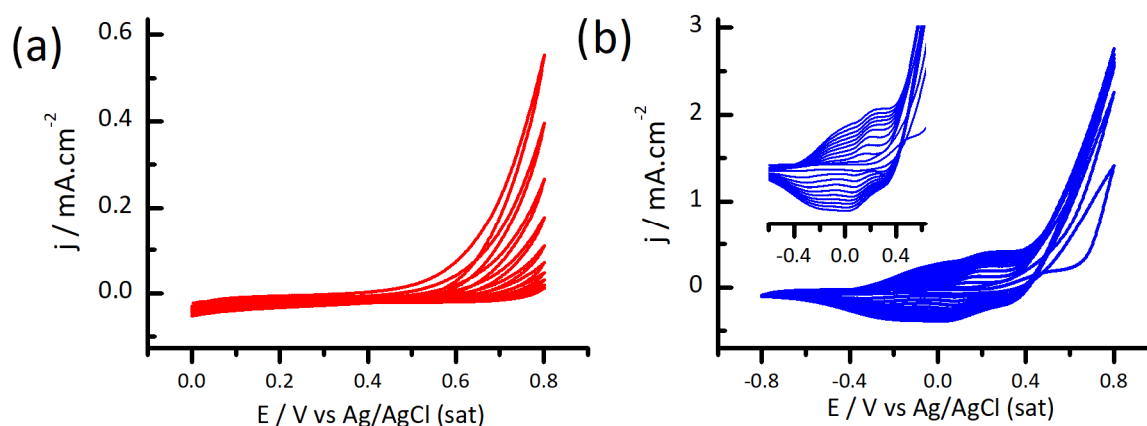


**Figure 1.** Cyclic voltammograms for solutions of (a) 150 mM PPY and (b) 150 mM PPY with 30 mM DA in PBS 7. The inset shows the presence of peaks in the region between  $-0.4$  and  $0.4$  V vs. Ag/AgCl (KCl sat). Scan rate:  $50 \text{ mV}\cdot\text{s}^{-1}$ .

### 3.2. Electrochemical Quartz Crystal Microbalance (eQCM) Studies of PPY-PDA Deposition

We next focused on the deposition of PPY-PDA films using the eQCM technique to follow the thickness of the deposited films by monitoring the mass deposited at the QCM surface as a function of fixed applied potential. Gold QCM chips (Seiko<sup>®</sup>) were utilised in these studies. Based on the CV results, an applied potential of  $0.85 \text{ V vs. Ag/AgCl (KCl, sat)}$  was chosen. Figure 2a shows a typical plot of the relative frequency shift over time for a gold chip modified with PPY-PDA. The chip surface was held at the open circuit potential (OCP) during equilibration before applying the voltage of  $0.85 \text{ V}$ . The resulting frequency shift was converted into an estimated film thickness (Figure 2b), as described in the methods section. These estimates were found to be broadly consistent with values derived from step profilometry of the deposited films (Figure S4). Assuming uniform thin-film deposition, PPY-PDA films were found to produce an average film thickness of more than twice that of pure PPY films deposited under identical conditions. This additional thickness was confirmed to be related to the extent of electropolymerisation by monitoring the charge passed ( $0.3 \text{ vs. } 0.17 \text{ C cm}^{-2}$  for PPY-PDA vs. PPY) during the potentiostatic step (Figure 2c). By repeating this experiment at least three times (full frequency traces are presented in the Supporting Information, Figure S3), the average growth rate in  $\text{nm/s}$  was estimated to be  $5 \pm 1 \text{ nm/s}$  for PPY compared to  $12 \pm 2 \text{ nm/s}$  for PPY-PDA (Figure 2d).

This significant enhancement in growth rate cannot be attributed to PDA deposition, as DA was found to electropolymerize slowly to produce films with a maximum of  $1\text{--}2 \text{ nm}$  diameter via cyclic voltammetry (Figure S1b). PDA auto-oxidation and electroless deposition due to intramolecular cyclisation reactions, producing dopaminechrome-like subunits (Scheme 1), can also be ruled out here as the pH remained neutral (pH 7) rather than showing the typical basic values required for spontaneous PDA formation [23]; moreover, no frequency shift due to PDA deposition is evident in Figure 1a or Figure S5 when the eQCM surface is kept at the OCP. We therefore conclude that the more rapid film deposition of PPY-PDA is due to the cooperative co-deposition of PDA within the PPY framework, resulting in a more rapid growth rate than either monomer achieves separately.

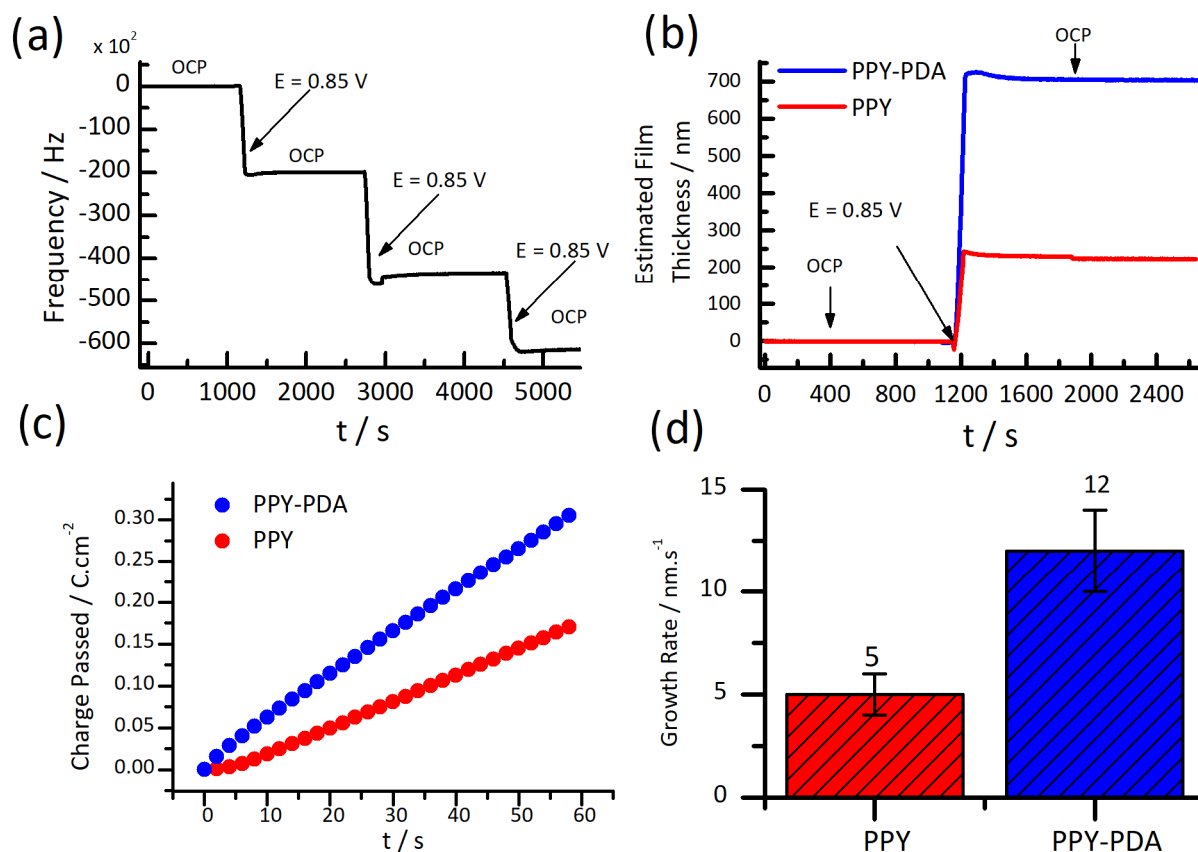


**Figure 2.** (a) Example frequency/time response of an eQCM chip in the presence of PY/DA solution at pH 7. The chip was first poised at the open circuit potential (OCP) prior to potentiostatic electropolymerisation steps at  $E = 0.85$  V vs. Ag/AgCl (KCl sat). The drop in resonant frequency with each step indicates the deposition of mass at the chip surface due to PPY-PDA film growth. (b) shows estimated film thicknesses following PPY and PPY-PDA deposition with identical step potentials and deposition times. The film growth is consistent with the greater charge passed for PPY-PDA films over the 60 s deposition, as shown in part (c). (d) Average estimated growth rates in nm/s for PPY and PPY-PDA films for at least 3 step potentials in each case.

### 3.3. Electrochemical Performance of PPY-PDA Coatings

While PDA films are known to have favourable biocompatibility and adhesive properties, pure PDA coatings are insulating and show a deterioration in charge transfer properties as the deposition thickness increases (Figure S1a). The incorporation of PDA into conductive PPY was therefore investigated as a strategy to prepare carbon-based electrodes with favourable charge transfer properties. Figure 3a shows voltammograms in a solution of 0.5 M KCl with 5 mM potassium hexacyanoferrate(III) (ferricyanide) on glassy carbon (GC) and GC modified with a 2 nm layer of PDA. Charge transfer to ferricyanide is totally inhibited by the PDA coating. By contrast, in Figure 3b, PPY-PDA coatings as thick as 600 nm show essentially unchanged peak-to-peak separation,  $\Delta E_p$ , despite the larger capacitive background current evident in the voltammograms. PPY-PDA coatings are therefore viable high-capacitance electrodes, incorporating some of the favourable properties of PDA without compromising interfacial charge transfer properties.

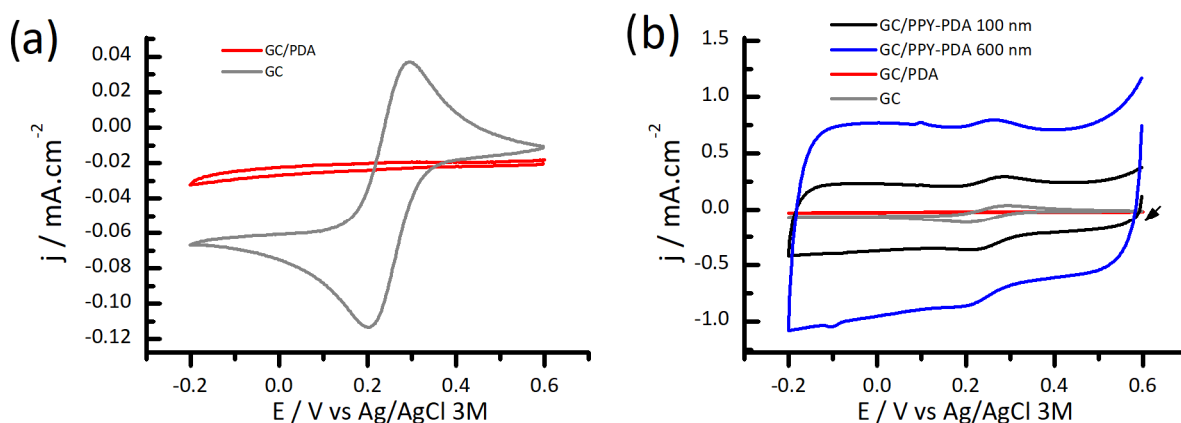


**Figure 3.** (a) Cyclic voltammograms in 5 mM potassium hexacyanoferrate(III) (ferricyanide) + 0.5 M KCl for glassy carbon (grey curve) and GC with a PDA coating. As PDA is insulating, the electrode is totally blocked for charge transfer after deposition of ca. 2 nm of PDA. (b) shows voltammograms in identical solutions for GC coated with PPY-PDA of different estimated film thicknesses. While the film capacitance increases with thicker coatings, charge transfer to ferricyanide remains unchanged, indicating that these coatings are non-insulating. GC and GC/PDA data from (a) are repeated in (b) to serve as a comparison. Scan rate:  $10 \text{ mV}\cdot\text{s}^{-1}$ .

#### 3.4. Morphology and Roughness of PPY and PPY-PDA Films by AFM and Water Contact Angle Measurements

The effects of PDA incorporation into the morphological and PPY-PDA films were investigated using a combination of AFM imaging and water contact angle measurements. The results are reported in Figure 4 and Table 1. Water contact angles for PPY and PDA between  $45^\circ$  and  $55^\circ$  on Au substrates are broadly consistent with previous reports [24]. However, significantly lower contact angles of around  $21^\circ$  were found for PPY-PDA films. This suggests significantly different surface free energy properties for the mixed films compared to pure PPY or PDA films.

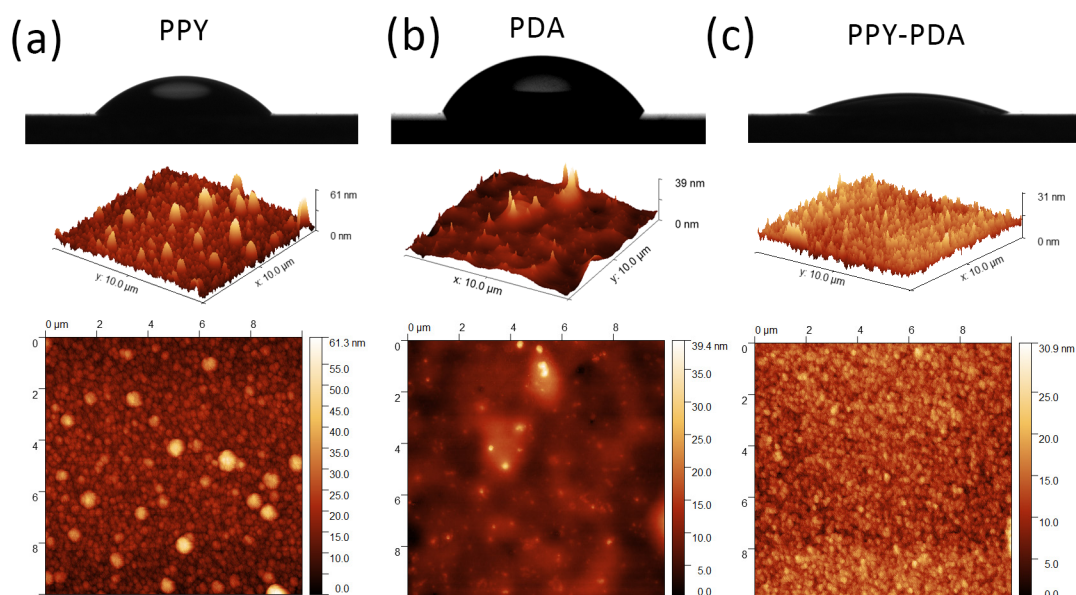


**Figure 4.** Water contact angle and AFM characterisation of (a) PPY, (b) PDA and (c) PPY-PDA coatings deposited on planar Au/Si electrodes.

**Table 1.** RMS Roughness values for PPY, PDA and PPY-PDA deposited on Au/Si electrodes. Values reported are mean  $\pm$  95% confidence interval.

Sample	Au	PPY	PDA	PPY-PDA
Roughness/nm	1.7 $\pm$ 0.2	4.9 $\pm$ 0.9	2.4 $\pm$ 0.7	3.2 $\pm$ 0.1
Water Contact Angle/ $^{\circ}$	>90	45 $\pm$ 1	54 $\pm$ 5	21.3 $\pm$ 0.9

AFM measurements on PPY (Figure 4a) show the presence of considerable agglomerates in the films, which have the effect of greatly increasing the RMS roughness (ca. 5 nm compared to 1.7 nm for the Au substrate). PDA films (Figure 4b) are considerably smoother (2.4 nm), but also show localised regions of agglomeration in the height profile. Only PPY-PDA (Figure 4c) shows a relatively homogeneous surface profile with a roughness value (3.2 nm) intermediate between that of pure PPY and PDA. Co-deposition of PDA within PPY therefore has the effects of both improving the film homogeneity and increasing hydrophilicity, both of which are important for application as electrodes.

### 3.5. Spectroscopic Characterisation of PPY and PPY-PDA Films

PPY and PPY-PDA films were characterised using a combination of FTIR (Figure 5a) and Raman spectroscopy (Figure 5b). Notable FTIR peaks include those at 1745 and 1700  $\text{cm}^{-1}$ , which are assigned to C-C=O and N-C=O species [25]. Peaks at 1535 and 1470  $\text{cm}^{-1}$  are attributed to C=C and C-N [26], as is the peak at 1286  $\text{cm}^{-1}$ . A clear peak at 1354  $\text{cm}^{-1}$  is present only in the PPY-PDA sample and is characteristic of indole C-N-C stretching modes, proving their presence in PPY-PDA [23]. This is further confirmed by FTIR analysis of PDA (Figure S6), which has similar peaks in the region between 1500–1200  $\text{cm}^{-1}$  assigned to both C-O and C-N groups [27].

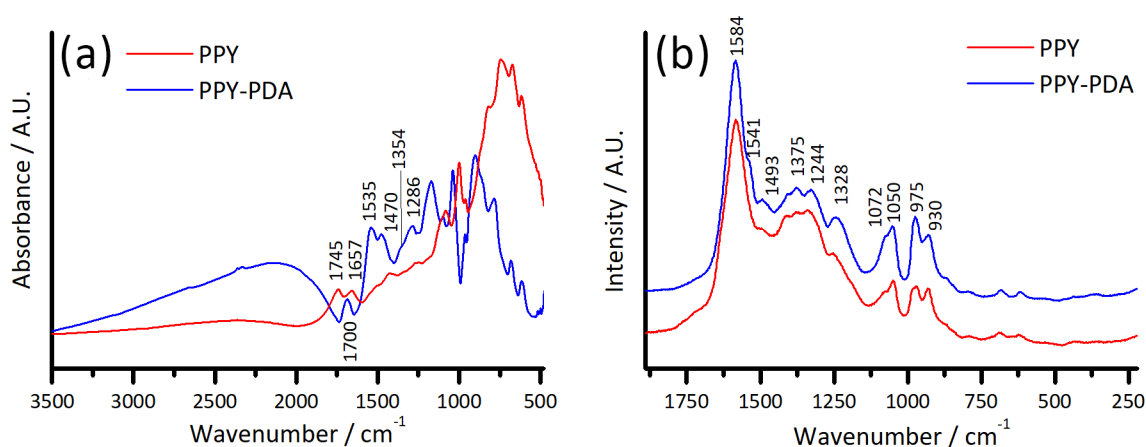


**Figure 5.** FTIR (a) and Raman (532 nm laser) spectra (b) of PPY and PPY-PDA films deposited on Au/Si substrates.

The Raman spectra support the notion that PPY and PPY-PDA films show a strongly ‘PPY-like’ structure, with modifications introduced by the presence of polydopamine-related structures in the scaffold. Most notably, the 1584  $\text{cm}^{-1}$  main peak is associated with C-C intercycle stretching and strongly correlated to the oxidation state of the polymer [28]. Peaks at 1375  $\text{cm}^{-1}$  are due to bipolaron ring stretching, while those at 1328  $\text{cm}^{-1}$  are due to polaron ring stretching, with similar attributions for peaks at 975 and 930  $\text{cm}^{-1}$  [29]. By contrast, the 1548  $\text{cm}^{-1}$  shoulder peak is only observed in PPY-PDA and this may be due to increasing levels of C=N in PPY-PDA due to the presence of PDA products [17].

The incorporation of PDA into PPY resulted in significant chemical modifications of the carbon film scaffold. These modifications were followed via XPS studies of PDA, PPY, and PDA deposited onto gold electrodes. Results are summarised in Figure 6 and S7. For PDA, the main contributions to the C 1s envelope (Figure 6a) are  $\text{CH}_x/\text{C-NH}_2$  centred

at 284.8 eV, C-O and C-N at 286 eV, C=O and C=N at 287.5 eV, O-C=O at 288.6 eV, and a  $\pi-\pi^*$  shake-up peak around 291 eV, consistent with previously reported studies of PDA via XPS [13,30]. In Figure 6b, the N 1s envelope comprises tertiary or aromatic, secondary, and primary amines at 398, 400.2, and 402.9 eV, respectively. The predominance of secondary amines is consistent with a mature PDA coating, wherein the majority of primary amines (e.g., present as polycatecholamines or DA monomers) participate in cyclisation reactions to form oligomers of dopaminechrome, some of which undergo aromatisation to yield imine-type products [13]. The N/C ratio (0.12) is also close to the expected value ( $\sim 0.1$ ) for PDA. O 1s deconvolution (Figure 6c) yielded a majority of C-O contributions from catechols at 533 eV and C=O from quinones at 531.4 eV.

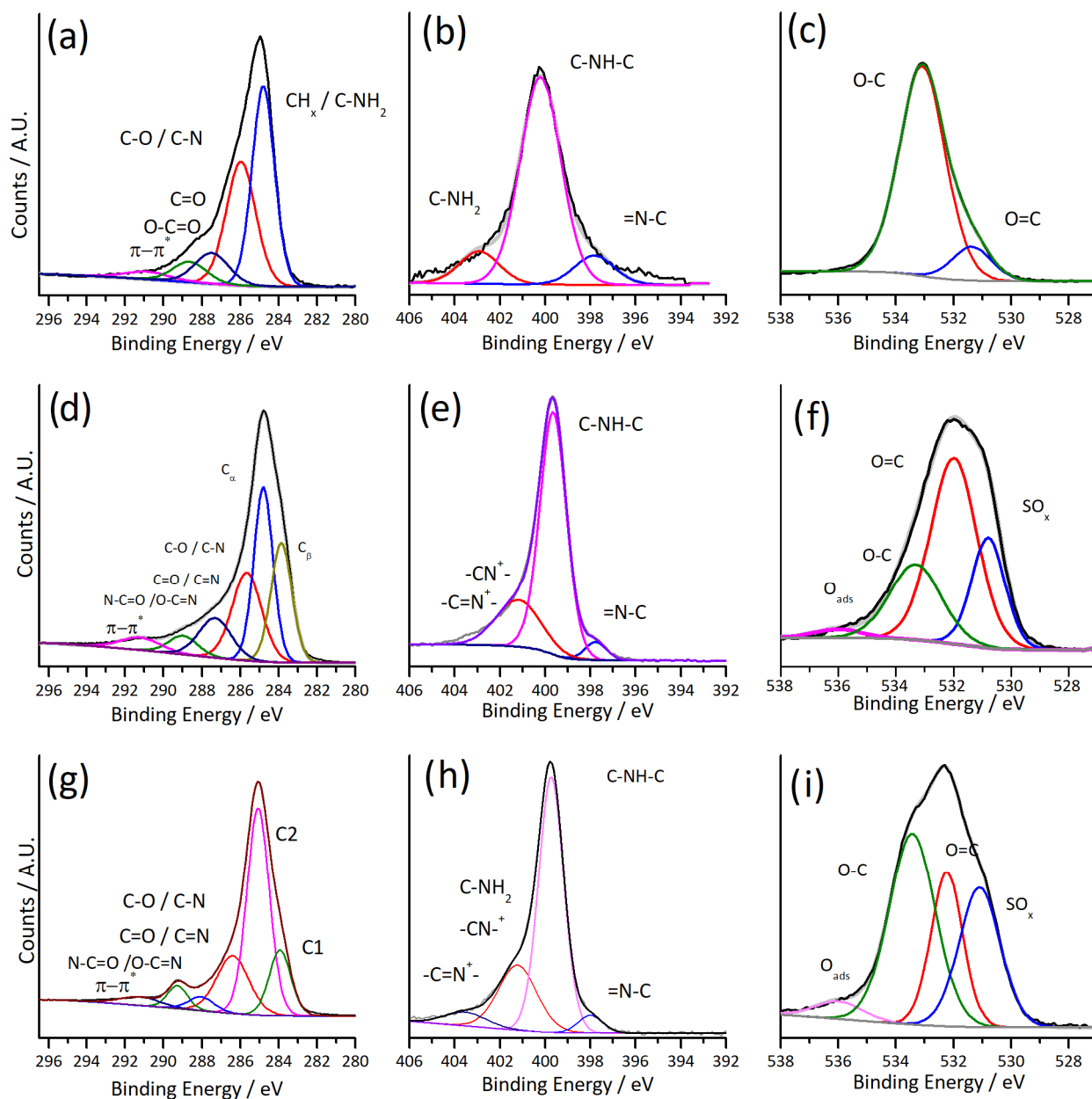


**Figure 6.** Deconvoluted XPS spectra for PDA (a–c), PPY (d–f) and PPY-PDA (g–i). C 1s spectra are presented in the leftmost column, N 1s spectra in the central column, and O 1s in the rightmost column of the figure.

Next, we characterised pure PPY films, in which the C 1s spectrum (Figure 6d) showed most of the same higher energy contributions above 285 eV as found for PDA, consistent with the fact the PPY films were left exposed to air prior to analysis and hence subject to passive oxidation [25]. In contrast to PDA, peaks at 284.9 and 284.0 were associated with the  $\alpha$  and  $\beta$  carbons of polypyrrole, respectively. For the N 1s spectrum (Figure 6e), =N-C and C-NH-C species were also evident at 398 and 400 eV, while a higher binding energy peak centred at 401 eV was associated with N+ species (polarons and bipolarons) [25,31]. Unlike pure PDA, the O 1s spectrum (Figure 6f) was predominantly (ca. 50%) O=C around 532 eV, with O-C at 533.3 eV and O<sub>ads</sub> at 536 eV [30]. Considering the presence of sulphur in the survey spectrum (Figure S7), the remaining O 1s peak at 530.8 eV arose from the incorporation of sulphates into deposited PPY due to H<sub>2</sub>SO<sub>4</sub> encountered in the electrolyte during deposition [31].

Considering the assignments of PDA and PPY, mixed PPY-PDA spectra in Figure 6g–i have peaks associated to both polymers, with predominantly PPY contributions. The full assignment (Table 2) has numerous ambiguities due to spectral overlap, but several notable peaks in each spectrum can be interpreted as arising from the presence of PDA and dopamine-related subunits in the mixed film. For instance, while it is difficult to differentiate peaks in the C 1s spectrum (Figure 6g) between 284–285 eV between CH<sub>x</sub>/C-NH<sub>2</sub> of PDA and the  $\alpha$  and  $\beta$  carbons of PPY, a higher contribution associated to O-C=O and similar species at 289 eV is clearly evident when comparing results to those in Figure 6d,g, which may be due to additional contributions of these species from PDA within the PPY-PDA scaffold.

**Table 2.** XPS peak assignments for PDA, PPY and PPY-PDA samples.

Sample	Contribution	C 1s		N 1s			O 1s		
		Position	At.%	Contribution	Position	At.%	Contribution	Position	At.%
PDA	CH <sub>x</sub>	284.8	43.81	R3N/Ar-N	397.8	10.86	C=O	531.36	12.19
	C-O/C-N	285.9	35.65	R2N-H	400.2	77.06	C-O	533.09	87.81
	C=O/C=N	287.5	10.26	RNH2	402.9	12.08			
	O-C=O	288.6	6.9						
	$\pi$ - $\pi^*$	290.8	3.37						
PPY	C $_{\beta}$	283.9	24.05	=N-C	398.1	6.75	SO42-	530.79	22.11
	C $_{\alpha}$	284.9	29.65	C-NH-C	399.7	50.12	C=O	531.99	52
	C-O and C-N	285.8	24.67	C-NH-C	400.3	18.65	C-O	533.32	23.45
	C=O and C=N	287.4	11.56	Polaron/Bipolaron	401.2	21.66	O <sub>ads</sub>	536	2.44
	O-C=O	288.9	5.12		403.4	2.82			
	$\pi$ - $\pi^*$	291.1	4.95						
PPY-PDA	CH <sub>x</sub> /C $_{\beta}$	283.9	15.61	=N-C	398	4.33	SO42-	530.84	29.16
	C $_{\alpha}$	285.1	51.19	C-NH-C	399.7	64.77	C=O	531.96	22.3
	C-O/C-N	286.4	20.4	Polaron/Bipolaron	401.2	25.13	C-O	533.14	44.26
	C=O/C=N	288.0	3.89		403.5	5.77	O <sub>ads</sub>	535.69	4.27
	O-C=O	289.3	5.06						
	$\pi$ - $\pi^*$	291.2	3.85						

The presence of PDA is most evident in the PPY-PDA O 1s spectrum in Figure 6i, in which O-C contributions at 533.2 eV now predominate over O=C as the major chemical species. This enhancement of O-C contributions is consistent with the abundant catechols associated with the presence of PDA within the mixed film and cannot only be associated with the oxidation of PPY, as this yields mostly O=C type species as evidenced in Figure 6f. We thus conclude that XPS data for PPY-PDA films are consistent with a PPY-like scaffold, with minor but significant contributions related to polymerised dopamine subunits.

### 3.6. Optoelectronic Properties of PPY and PPY-PDA Films

XPS provides invaluable information on the surface chemical properties of the PPY and PPY-PDA films, but it is also important to understand how bulk electrode properties are affected by the co-incorporation of PDA. Electrodes prepared from PPY and related conjugated polymer films often have their optical properties characterised by the optical (Tauc) gap [32,33]. The Tauc formulation relates the band gap of a semiconductor material to its absorption coefficient, according to the Tauc equation [34]:

$$(\alpha \cdot h\nu)^n = K(h\nu - E_g)$$

where  $\alpha$  is the absorption coefficient,  $h\nu$  is the photon energy, and  $E_g$  is the band gap. The exponent  $n$  varies according to the type of transition:  $n = \frac{1}{2}$  describes direct transitions, while  $n = 2$  describes allowed indirect transitions and is more regularly applied to PPY and related materials [35,36]. Absorbance spectra for PPY-PDA and PPY films deposited on ITO are shown in Figure 7a. These data were used to derive  $\alpha$  values according to

$$\alpha = 2.303 A/t$$

with  $A$  the absorbance and  $t$  the film thickness. The resulting Tauc plots for PPY (Figure 7a) and PPY-PDA (Figure 7b) yielded optical gaps of ca. 2.1 eV for both PPY and PPY-PDA. These values are consistent with previous reports [36] and suggest that PDA incorporation into PPY films does not dramatically alter the bulk optoelectronic properties of the deposited films.

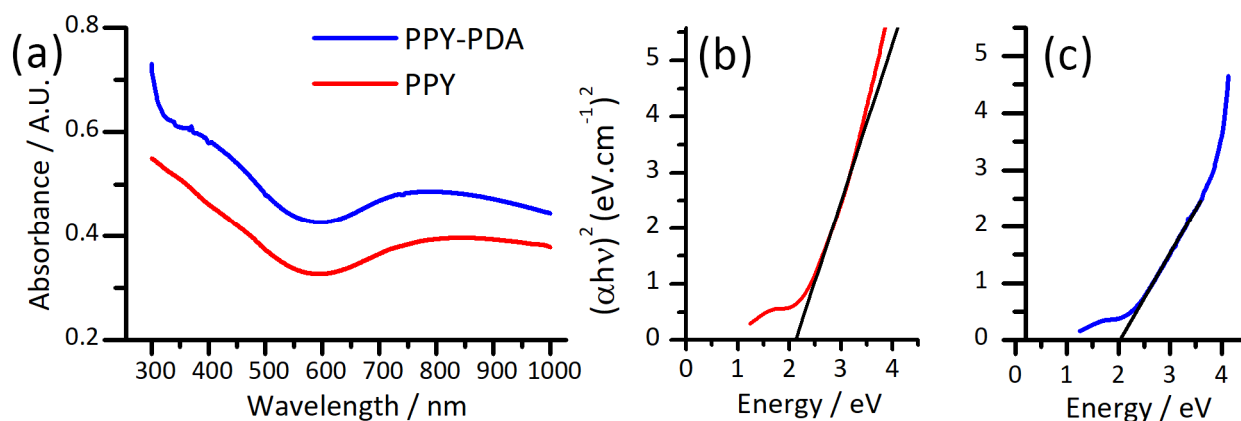


**Figure 7.** (a) UV-vis spectra of PPY and PPY-PDA deposited on ITO electrodes. Tauc plots for (b) PPY and (c) PPY-PDA derived from absorbance data. The Tauc gap was estimated by the line of best fit to the linear region of the plots extrapolated to the  $x$ -axis (black lines).

## 4. Discussion and Conclusions

PDA has previously been observed to improve the adhesive properties of electrodeposited PPY films and to increase the apparent rate of film electrodeposition. Here, we have for the first time systematically and quantitatively investigated the effects of the presence of PDA in solution during PPY electrodeposition, using a combination of spectroscopic methods, electrochemical analysis, electrochemical quartz crystal microbalance studies, and morphological analysis via AFM. The introduction of PDA as a minor component during PPY electrodeposition both lowers the required potential for significant electropolymerisation to occur and more than doubles the growth rate of the resulting films during potentiostatic deposition, as evidenced by eQCM studies.

The characterisation of the resulting films by XPS, FTIR, Raman, and UV-vis spectroscopy proves that the films have a predominant ‘PPY-like’ character, with no noted change in the observed optical (Tauc) gap serving as key evidence that the bulk structure of the films is not substantially changed by PDA incorporation. This is also consistent with

the charge transfer studies of the films, which show increased capacitance compared to unmodified electrodes, but similar  $\Delta E_p$  values for charge transfer to ferricyanide for both PPY and PPY-PDA. Hence, while pure PDA is a known insulator, its incorporation into PPY preserves film conductivity and bulk structure.

Taken together with the evidence of PDA-like structures in PPY-PDA from XPS, FTIR, and Raman studies, this suggests that these PDA structures (for example, derivatives of dopaminechrome oligomers [13]) are dispersed throughout a scaffold with a predominant PPY character. Considering the lower measured onset potential for dopamine oxidation and electropolymerisation (ca. 0.4 V vs. Ag/AgCl (KCl sat) at pH 7 in Figure S1) compared to the initial onset of PPY electrodeposition at potentials > 0.7 V vs. Ag/AgCl (KCl sat), we propose a simple 2-step model whereby the initial PDA oligomerisation at the electrode surface induced at lower applied potentials serve as the nuclei for rapid PPY electropolymerisation and precipitation. This model is consistent with models of PDA formation, which have an initial nucleation of oligomers in solution [37], and would explain why such films retain the characteristic adhesiveness of PDA across all electrode surfaces tested without resulting in the development of an extensive non-conductive PDA film. Importantly, as auto-oxidation and polymerisation of dopamine was ruled out under our experimental conditions (Figure 2a), the resulting PPY-PDA film growth was determined only via the applied potential.

Finally, PDA incorporation significantly alters the morphology of PPY-PDA compared to 'pure' films, as evident in AFM studies (Figure 3). The roughness of PPY-PDA is intermediate between that of PPY and PDA only, and the film surface is evidently more homogeneous with no large agglomerates of material as displayed by PPY only (Figure 3a). Considering the evidence of PDA-like domains in the material from spectroscopic data, these data suggest a PPY-like structure peppered with frequent (but not necessarily interconnected) PDA regions, which in turn alters the morphology of the material while preserving its predominant PPY character. This morphology, as well as the presence of abundant catechol groups (evidenced by XPS, Figure 3), may explain the lower water contact angle of PPY-PDA compared to either pure film.

PDA incorporation into PPY is therefore a viable strategy for universal conductive film growth across any conductive surface, while also allowing researchers to retain control of interfacial properties and surface chemistry, both of which are key for tuning biocompatibility and redox properties.

**Supplementary Materials:** The following supporting information can be downloaded at: <https://www.mdpi.com/article/10.3390/c10010020/s1>, Figure S1: Electrodeposition of polydopamine (PDA) investigation by eQCM. Figure S2: Images of coherent adhesive PPY-PDA coatings on ITO glass and gold electrodes. Figure S3: Comparison of PPY and PPY-PDA electrodeposition by CV on ITO. Figure S4: Profilometry of PPY and PPY-PDA films. Figure S5: Frequency-time curves for potentiostatic deposition of PPY and PPY-PDA via eQCM. Figure S6: FTIR spectra of PDA and dopamine hydrochloride. Figure S7: supplementary XPS data.

**Author Contributions:** Conceptualization, J.A.B.; methodology, J.A.B.; validation, J.A.B. and F.B.; formal analysis, J.A.B.; investigation, J.A.B.; resources, F.B.; data curation, J.A.B. and F.B.; writing—original draft preparation, J.A.B.; writing—review and editing, J.A.B. and F.B.; visualization, J.A.B.; supervision, F.B.; project administration, F.B.; funding acquisition, J.A.B. and F.B. All authors have read and agreed to the published version of the manuscript.

**Funding:** This project has received funding from the European Union's Horizon 2020 research and innovation programme under the Marie Skłodowska-Curie grant agreement No 899546. This study was also supported by the French National Research Agency under grant number 19-CE43-0013-01, CATHOMIX.

**Data Availability Statement:** Data will be made available upon request.

**Acknowledgments:** The authors are grateful to A. Moréac and G. Taupier of the Institute de Physique de Rennes for carrying out Raman analysis. We acknowledge the ASPHERYX platform from ScanMAT, UAR 2025 Université de Rennes-CNRS (CPER MAT&Trans 2021-2027) for XPS studies and are grateful to Corinne Lagrost for carrying out the XPS analysis.

**Conflicts of Interest:** The authors declare no conflicts of interest.

## References

1. Asavapiriyant, S.; Chandler, G.K.; Gunawardena, G.A.; Pletcher, D. The Electrodeposition of Polypyrrole Films from Aqueous Solutions. *J. Electroanal. Chem. Interfacial Electrochem.* **1984**, *177*, 229–244. [[CrossRef](#)]
2. Sabouraud, G.; Sadki, S.; Brodie, N. The Mechanisms of Pyrrole Electropolymerization. *Chem. Soc. Rev.* **2000**, *29*, 283–293. [[CrossRef](#)]
3. Ramanaviciene, A.; Ramanavicius, A. Application of Polypyrrole for the Creation of Immunosensors. *Crit. Rev. Anal. Chem.* **2002**, *32*, 245–252. [[CrossRef](#)]
4. Ateh, D.D.; Navsaria, H.A.; Vadgama, P. Polypyrrole-Based Conducting Polymers and Interactions with Biological Tissues. *J. R. Soc. Interface* **2006**, *3*, 741–752. [[CrossRef](#)]
5. Huang, Y.; Li, H.; Wang, Z.; Zhu, M.; Pei, Z.; Xue, Q.; Huang, Y.; Zhi, C. Nanostructured Polypyrrole as a Flexible Electrode Material of Supercapacitor. *Nano Energy* **2016**, *22*, 422–438. [[CrossRef](#)]
6. Choudhary, R.B.; Ansari, S.; Purty, B. Robust Electrochemical Performance of Polypyrrole (PPy) and Polyindole (PIn) Based Hybrid Electrode Materials for Supercapacitor Application: A Review. *J. Energy Storage* **2020**, *29*, 101302. [[CrossRef](#)]
7. Fabregat, G.; Córdova-Mateo, E.; Armelin, E.; Bertran, O.; Alemán, C. Ultrathin Films of Polypyrrole Derivatives for Dopamine Detection. *J. Phys. Chem. C* **2011**, *115*, 14933–14941. [[CrossRef](#)]
8. Jain, R.; Jadon, N.; Pawaiya, A. Polypyrrole Based next Generation Electrochemical Sensors and Biosensors: A Review. *TrAC Trends Anal. Chem.* **2017**, *97*, 363–373. [[CrossRef](#)]
9. Andriukonis, E.; Reinikovaite, V.; Ramanavicius, A. Comparative Study of Polydopamine and Polypyrrole Modified Yeast Cells Applied in Biofuel Cell Design. *Sustain. Energy Fuels* **2022**, *6*, 4209–4217. [[CrossRef](#)]
10. Yuan, X.; Ding, X.-L.; Wang, C.-Y.; Ma, Z.-F. Use of Polypyrrole in Catalysts for Low Temperature Fuel Cells. *Energy Environ. Sci.* **2013**, *6*, 1105–1124. [[CrossRef](#)]
11. Kim, M.; Li, S.; Kong, D.S.; Song, Y.E.; Park, S.-Y.; Kim, H.; Jae, J.; Chung, I.; Kim, J.R. Polydopamine/Polypyrrole-Modified Graphite Felt Enhances Biocompatibility for Electroactive Bacteria and Power Density of Microbial Fuel Cell. *Chemosphere* **2023**, *313*, 137388. [[CrossRef](#)]
12. Kim, S.; Jang, L.K.; Park, H.S.; Lee, J.Y. Electrochemical Deposition of Conductive and Adhesive Polypyrrole-Dopamine Films. *Sci. Rep.* **2016**, *6*, 30475. [[CrossRef](#)]
13. Hemmatpour, H.; De Luca, O.; Crestani, D.; Stuart, M.C.A.; Lasorsa, A.; van der Wel, P.C.A.; Loos, K.; Gioussis, T.; Haddadi-Asl, V.; Rudolf, P. New Insights in Polydopamine Formation via Surface Adsorption. *Nat. Commun.* **2023**, *14*, 664. [[CrossRef](#)] [[PubMed](#)]
14. Kim, S.; Lee, S.; Park, J.; Lee, J.Y. Electrochemical Co-Deposition of Polydopamine/Hyaluronic Acid for Anti-Biofouling Bioelectrodes. *Front. Chem.* **2019**, *7*, 262. [[CrossRef](#)]
15. Kim, J.H.; Lee, M.; Park, C.B. Polydopamine as a Biomimetic Electron Gate for Artificial Photosynthesis. *Angew. Chem. Int. Ed.* **2014**, *53*, 6364–6368. [[CrossRef](#)] [[PubMed](#)]
16. Kang, S.M.; You, I.; Cho, W.K.; Shon, H.K.; Lee, T.G.; Choi, I.S.; Karp, J.M.; Lee, H. One-Step Modification of Superhydrophobic Surfaces by a Mussel-Inspired Polymer Coating. *Angew. Chem. Int. Ed.* **2010**, *49*, 9401–9404. [[CrossRef](#)] [[PubMed](#)]
17. Geng, H.; Lupton, E.J.; Ma, Y.; Sun, R.; Grigsby, C.L.; Brachi, G.; Li, X.; Zhou, K.; Stuckey, D.J.; Stevens, M.M. Hybrid Polypyrrole and Polydopamine Nanosheets for Precise Raman/Photoacoustic Imaging and Photothermal Therapy. *Adv. Healthc. Mater.* **2023**, *12*, e2301148. [[CrossRef](#)] [[PubMed](#)]
18. Zhang, W.; Yang, F.K.; Pan, Z.; Zhang, J.; Zhao, B. Bio-Inspired Dopamine Functionalization of Polypyrrole for Improved Adhesion and Conductivity. *Macromol. Rapid Commun.* **2014**, *35*, 350–354. [[CrossRef](#)]
19. Behan, J.A.; Grajkowski, F.; Jayasundara, D.R.; Vilella-Arribas, L.; García-Melchor, M.; Colavita, P.E. Influence of Carbon Nanostructure and Oxygen Moieties on Dopamine Adsorption and Charge Transfer Kinetics at Glassy Carbon Surfaces. *Electrochim. Acta* **2019**, *304*, 221–230. [[CrossRef](#)]
20. Ait-Itto, F.-Z.; Behan, J.A.; Martinez, M.; Barrière, F. Development of Bioanodes Rich in Exoelectrogenic Bacteria Using Iron-Rich Palaeomarine Sediment Inoculum. *Bioelectrochemistry* **2024**, *156*, 108618. [[CrossRef](#)]
21. Huang, X.; Chen, Q.; Pan, W.; Yao, Y. Advances in the Mass Sensitivity Distribution of Quartz Crystal Microbalances: A Review. *Sensors* **2022**, *22*, 5112. [[CrossRef](#)]
22. Diaz, A.F.; Castillo, J.I.; Logan, J.A.; Lee, W.-Y. Electrochemistry of Conducting Polypyrrole Films. *J. Electroanal. Chem. Interfacial Electrochem.* **1981**, *129*, 115–132. [[CrossRef](#)]
23. Zangmeister, R.A.; Morris, T.A.; Tarlov, M.J. Characterization of Polydopamine Thin Films Deposited at Short Times by Autoxidation of Dopamine. *Langmuir* **2013**, *29*, 8619–8628. [[CrossRef](#)]

24. Ball, V.; Del Frari, D.; Michel, M.; Buehler, M.J.; Toniazzo, V.; Singh, M.K.; Gracio, J.; Ruch, D. Deposition Mechanism and Properties of Thin Polydopamine Films for High Added Value Applications in Surface Science at the Nanoscale. *BioNanoScience* **2012**, *2*, 16–34. [[CrossRef](#)]
25. Tabačiarová, J.; Mičušík, M.; Fedorko, P.; Omastová, M. Study of Polypyrrole Aging by XPS, FTIR and Conductivity Measurements. *Polym. Degrad. Stab.* **2015**, *120*, 392–401. [[CrossRef](#)]
26. Khadem, F.; Pishvaei, M.; Salami-Kalajahi, M.; Najafi, F. Morphology Control of Conducting Polypyrrole Nanostructures via Operational Conditions in the Emulsion Polymerization. *J. Appl. Polym. Sci.* **2017**, *134*, 44697. [[CrossRef](#)]
27. Mallinson, D.; Mullen, A.B.; Lamprou, D.A. Probing Polydopamine Adhesion to Protein and Polymer Films: Microscopic and Spectroscopic Evaluation. *J. Mater. Sci.* **2018**, *53*, 3198–3209. [[CrossRef](#)]
28. Nguyen Thi Le, H.; Bernard, M.C.; Garcia-Renaud, B.; Deslouis, C. Raman Spectroscopy Analysis of Polypyrrole Films as Protective Coatings on Iron. *Synth. Met.* **2004**, *140*, 287–293. [[CrossRef](#)]
29. Morávková, Z.; Taboubi, O.; Minisy, I.M.; Bober, P. The Evolution of the Molecular Structure of Polypyrrole during Chemical Polymerization. *Synth. Met.* **2021**, *271*, 116608. [[CrossRef](#)]
30. Rella, S.; Mazzotta, E.; Caroli, A.; De Luca, M.; Bucci, C.; Malitesta, C. Investigation of Polydopamine Coatings by X-Ray Photoelectron Spectroscopy as an Effective Tool for Improving Biomolecule Conjugation. *Appl. Surf. Sci.* **2018**, *447*, 31–39. [[CrossRef](#)]
31. Idla, K.; Talo, A.; Niemi, H.E.-M.; Forsén, O.; Yläsaari, S. An XPS and AFM Study of Polypyrrole Coating on Mild Steel. *Surf. Interface Anal.* **1997**, *25*, 837–854. [[CrossRef](#)]
32. Behan, J.A.; Stamatina, S.N.; Hoque, M.K.; Ciapetti, G.; Zen, F.; Esteban-Tejeda, L.; Colavita, P.E. Combined Optoelectronic and Electrochemical Study of Nitrogenated Carbon Electrodes. *J. Phys. Chem. C* **2017**, *121*, 6596–6604. [[CrossRef](#)]
33. Zen, F.; Karanikolas, V.D.; Behan, J.A.; Andersson, J.; Ciapetti, G.; Bradley, A.L.; Colavita, P.E. Nanoplasmonic Sensing at the Carbon-Bio Interface: Study of Protein Adsorption at Graphitic and Hydrogenated Carbon Surfaces. *Langmuir* **2017**, *33*, 4198–4206. [[CrossRef](#)] [[PubMed](#)]
34. Makuła, P.; Pacia, M.; Macyk, W. How To Correctly Determine the Band Gap Energy of Modified Semiconductor Photocatalysts Based on UV–Vis Spectra. *J. Phys. Chem. Lett.* **2018**, *9*, 6814–6817. [[CrossRef](#)] [[PubMed](#)]
35. Gonçalves, R.; Paiva, R.S.; Ramirez, A.M.R.; Mwanda, J.A.; Pereira, E.C.; Cuesta, A. Mapping the Electronic Structure of Polypyrrole with Image-Based Electrochemical Scanning Tunneling Spectroscopy. *Electrochem. Sci. Adv.* **2022**, *2*, e2100028. [[CrossRef](#)]
36. Abdi, M.M.; Ekramul Mahmud, H.N.M.; Abdullah, L.C.; Kassim, A.; Zaki Ab. Rahman, M.; Chyi, J.L.Y. Optical Band Gap and Conductivity Measurements of Polypyrrole-Chitosan Composite Thin Films. *Chin. J. Polym. Sci.* **2012**, *30*, 93–100. [[CrossRef](#)]
37. Alfieri, M.L.; Micillo, R.; Panzella, L.; Crescenzi, O.; Oscurato, S.L.; Maddalena, P.; Napolitano, A.; Ball, V.; d’Ischia, M. Structural Basis of Polydopamine Film Formation: Probing 5,6-Dihydroxyindole-Based Eumelanin Type Units and the Porphyrin Issue. *ACS Appl. Mater. Interfaces* **2018**, *10*, 7670–7680. [[CrossRef](#)]

**Disclaimer/Publisher’s Note:** The statements, opinions and data contained in all publications are solely those of the individual author(s) and contributor(s) and not of MDPI and/or the editor(s). MDPI and/or the editor(s) disclaim responsibility for any injury to people or property resulting from any ideas, methods, instructions or products referred to in the content.